

www.advenergymat.de

Understanding the Outstanding High-Voltage Performance of NCM523||Graphite Lithium Ion Cells after Elimination of **Ethylene Carbonate Solvent from Conventional Electrolyte**

Sven Klein, Stefan van Wickeren, Stephan Röser, Peer Bärmann, Kristina Borzutzki, Bastian Heidrich, Markus Börner, Martin Winter,* Tobias Placke,* and Johannes Kasnatscheew*

The increase of specific energy of current Li ion batteries via further increase of the cell voltage, for example, to 4.5 V is typically accompanied by a sudden and rapid capacity fade, known as "rollover" failure. This failure is the result of Li dendrite formation triggered in the course of electrode cross-talk, that is, dissolution of transition metals (TMs) from the cathode and deposition on the anode. It is shown herein, that the elimination of ethylene carbonate (EC) from a state-of-theart electrolyte, that is, from 1.0 M LiPF₆ in a 3:7 mixture of EC and ethyl methyl carbonate prevents this failure in high-voltage LiNi_{0.5}Co_{0.2}Mn_{0.3}O₂||graphite cells, even without any electrolyte additives. While the oxidative stability on the cathode side is similar in both electrolytes, visible by a decomposition plateau at 5.5 V versus Li|Li+ during charge, the anode side in the EC-free electrolyte reveals significantly less TM deposits and Li metal dendrites compared to the EC-based electrolyte. The beneficial effect of EC-free electrolytes is related to a significantly increased amount of degraded LiPF₆ species, which effectively trap dissolved TMs and suppress the effect of detrimental cross-talk, finally realizing rolloverfree performance under high voltage conditions.

S. Klein, S. van Wickeren, Dr. S. Röser, P. Bärmann, B. Heidrich, Dr. M. Börner, Prof. M. Winter, Dr. T. Placke MEET Battery Research Center Institute of Physical Chemistry University of Münster Corrensstraße 46, 48149 Münster, Germany E-mail: tobias.placke@uni-muenster.de Dr. S. Röser E-Lyte Innovations GmbH Mendelstraße 11, 48149 Münster, Germany Dr. K. Borzutzki, Prof. M. Winter, Dr. J. Kasnatscheew

Helmholtz-Institute Münster **IEK-12**

Forschungszentrum Jülich GmbH Corrensstraße 46, 48149 Münster, Germany E-mail: m.winter@fz-juelich.de; j.kasnatscheew@fz.juelich.de

The ORCID identification number(s) for the author(s) of this article can be found under https://doi.org/10.1002/aenm.202003738.

© 2021 The Authors. Advanced Energy Materials published by Wiley-VCH GmbH. This is an open access article under the terms of the Creative Commons Attribution-NonCommercial-NoDerivs License, which permits use and distribution in any medium, provided the original work is properly cited, the use is non-commercial and no modifications or adaptations are made.

DOI: 10.1002/aenm.202003738

1. Introduction

The specific energy and energy density of state-of-the-art (SOTA) Li ion batteries (LIBs) can be further enhanced by increasing the charge voltage of the cell.[1-^{3]} However, accompanied decrease in cycle life and safety renders this approach challenging.[4]

The challenge is frequently related with the SOTA cathodes, which are based on layered oxide structures, for example, $LiNi_{0.5}Co_{0.2}Mn_{0.3}O_2$ (NCM523).^[5-7] On the one hand, they are thermodynamically unstable beyond a certain delithiation amount, that is, beyond a certain cathode charge potential (e.g., >4.3 V versus Li|Li⁺), which lead to performance-limiting phase changes. On the other hand, these cathode phase changes are intertwined with dissolution of transition metals (TMs), which in turn can affect the graphite-based anode in

the course of the well-known cross-talk (TM transport to anode and deposition there) and result in significant alteration of the solid electrolyte interphase (SEI) and irreversible consumption of active Li, thus available cell capacity. [8-16] In the worst case, high-voltage operation of NCM-based LIB cells (e.g., at cell voltages of 4.5 V) results in fast and significant capacity fading, which is often referred to as "rollover" failure, and has been observed in different studies. [9-11,17-19] In our previous publication,[20] we reported on the underlying mechanism for the rapid cell failure of high-voltage LIB cells, which can be attributed to severe SEI alteration at the graphite anode, due to deposited TMs migrating from the cathode to the anode, which in turn induce the formation of Li metal dendrites.

It is well-known that the electrolyte can significantly impact LIB performance and mitigate its fading, for example, via modifying the SEI layer on graphite-based negative electrode, [21-24] or via scavenging parasitic species, for example, TMs. The SOTA electrolyte typically consists of 1.0 M LiPF₆ in a solvent mixture of cyclic and linear carbonates, that is, ethylene carbonate (EC) and, for example, ethyl methyl carbonate (EMC).[25] While the linear carbonate component increases the fluidity (low viscosity) of the electrolyte, the cyclic carbonate increases the salt dissociation (high permittivity) and additionally decreases the highest occupied molecular orbital



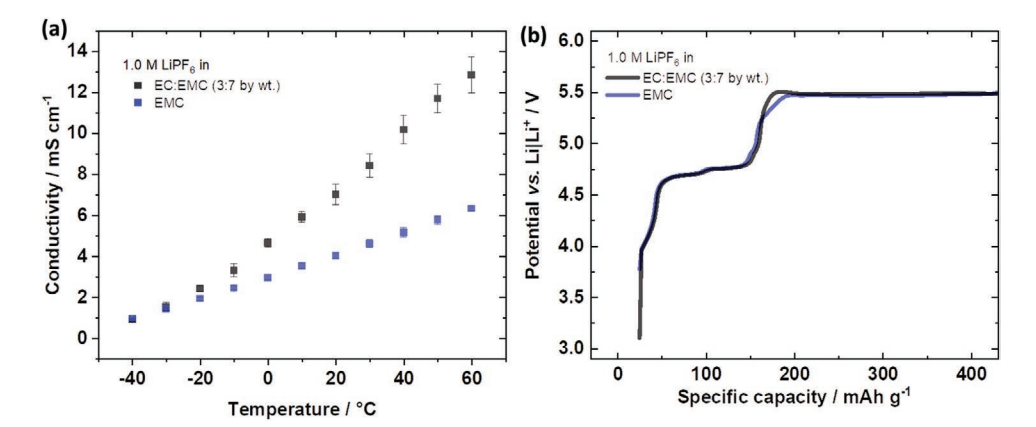


Figure 1. a) Ionic conductivities as a function of temperature for the EC-based and EC-free electrolytes, both revealing sufficient conductivities at 20 °C. b) Galvanostatic overcharge of LNMO electrodes for EC-based and EC-free electrolyte. Similar decomposition plateaus, thus, similar anodic stabilities up to 5.5. V versus LilLi+ are observed for both electrolytes.

of the electrolyte by strong Li⁺ coordination, thus overall results in an apparent synergistic electrolyte blend with maximized ionic conductivity and anodic stability, respectively.^[25,26]

Nevertheless, recent studies questioned the vital role of EC for LIB cells. The so-called "EC-free" electrolytes, based on, for example, EMC as the single solvent, also operate in various NCM||graphite cells even with apparent advantages in terms of high voltage applications (up to 4.5 V) and thermal stability.\[^{27-33}\] Nevertheless, these studies still contain small amounts of electrolyte additives (e.g., fluoroethylene carbonate, vinylene carbonate) and/or are performed at elevated temperatures (e.g., 40 °C), which renders a derivation of the underlying mechanism of entirely EC-free electrolytes difficult. In this work, this mechanism is systematically elaborated in NCM523||graphite cells at 20 °C without the use of any electrolyte additives at high voltage, that is, 4.5 V.

2. Results and Discussion

The ionic conductivities of SOTA electrolyte, that is, 1.0 m LiPF $_6$ in the solvent mixture based on cyclic EC and linear EMC are

compared with the EC-free electrolyte, that is, 1.0 m LiPF₆ in EMC (**Figure 1**a). The difference in ionic conductivities gets lower with decreasing temperature and is even similar below $-30~^{\circ}\text{C}$. Despite the low permittivity of the EC-free electrolyte, the ionic conductivities are still sufficient for application, that is, $\approx 4~\text{mS}~\text{cm}^{-1}$ at room temperature (20 °C). $^{[30,34]}$

The anodic stability, as another essential physicochemical requirement for electrolytes, [35] is depicted in Figure 1b for application-relevant conditions, that is, on Ni-containing and high voltage suitable composite electrode like LiNi_{0.5}Mn_{1.5}O₄ (LNMO) during galvanostatic overcharge. [36,37] Above the characteristic delithiation process of LNMO at 4.7–4.9 V versus Li|Li⁺, both electrolytes reveal similar high decomposition plateaus at 5.5 V versus Li|Li⁺. Independent of the EC content, both electrolytes are similarly stable under high-voltage application and the assumed vital role of EC in terms of anodic stability can be questioned. [26]

The voltage profiles of the electrolytes in NCM523||graphite full cells are depicted in **Figure 2**b for a charge cut-off voltage of 4.5 V. The EC-free electrolyte shows a slightly different charge behavior, that is, slight plateau at \approx 3.3 V and increased specific charge capacity by 7.6 mAh g⁻¹ (in total 233.4 mAh g⁻¹).

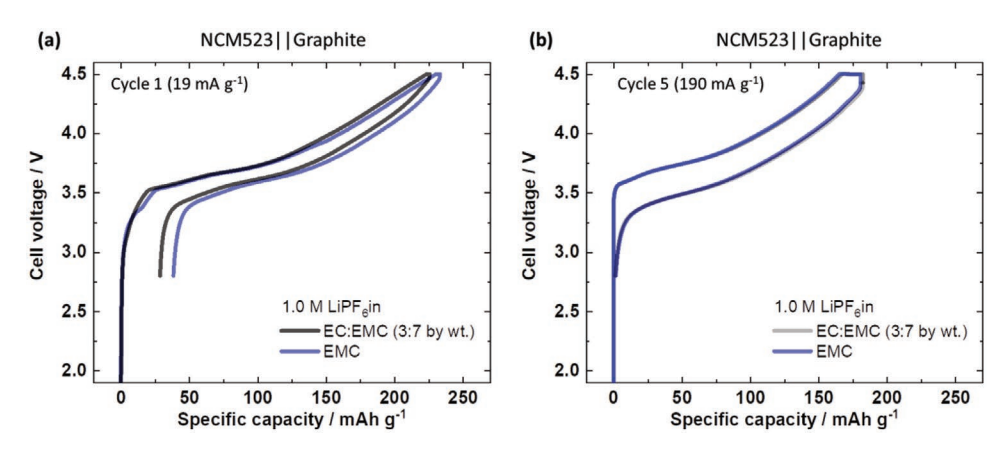


Figure 2. a) Cell voltage profiles of the initial charge/discharge cycle for EC-based and EC-free electrolytes in NMC523||graphite cells charged up to 4.5 V (0.1 C = 19 mA g^{-1}). The slight difference during the charge process points to differences in SEI formation at the graphite-based anode. b) Cell voltage profile of the fifth cycle with increased specific current (1 C = 190 mA g^{-1}). Similar specific capacities and even voltage hystereses demonstrate similar charge/discharge cycle performance for both electrolytes.

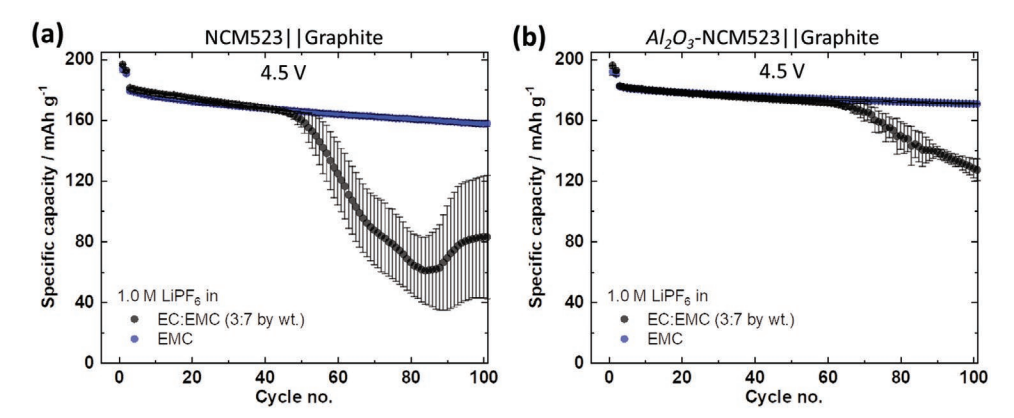


Figure 3. Charge/discharge cycling of a) NCM523||graphite full-cells and b) Al₂O₃-NCM523 ||graphite full-cells using EC-containing and EC-free electrolytes (2.8–4.5 V). Surface modification cannot prevent the rollover fading for the EC-based electrolyte while the EC-free electrolyte-based cells perform without this failure.

This difference can be related with a potential shift of the electrodes due to an altered potential of graphite-based anode in the course of different SEI formations. [24,38] After this formation, the performance is comparable for both electrolytes, as shown in Figure 2b for the fifth cycle. Similar specific capacities, overvoltages, and voltage hystereses demonstrate a similar initial performance implying a similar stable SEI, independent of the electrolyte, that is, independent of the presence of EC.

Despite initial similarity, significant differences evolve during long-term charge/discharge cycling, as shown in **Figure 3a**. In line with previous literature, the SOTA, that is, EC-containing electrolyte, is not suitable for high voltage application as it suffers from sudden and severe capacity decay (here: at cycle no. 45), which is known as rollover fading. Interestingly, such failure is absent for the electrolyte without EC. It is known, that the roll-over fading is the result of the electrode cross-talk, that is, TM dissolution from the cathode and transport to and deposition on the anode. In the cathode, as obvious initiator of this failure, can be modified by, for example, literature well-known coating with Al_2O_3 . Indeed the coating can prolong

the cycle life but still cannot prevent the sudden roll-over fading (here: cycle no. 65) as shown in Figure 3b, while the EC-free electrolyte, again, performs without this failure. Given the slightly better performance, the Al_2O_3 -NCM523-based CAM is used for upcoming mechanistic investigations.

Alterations of the graphite|electrolyte interface as another possibility for the observed performance difference is investigated by means of scanning electron microscopy (SEM) combined with the energy dispersive X-ray (EDX) technique of graphite after 100 charge/discharge cycles and are depicted in **Figure 4**. In fact, for EC-containing electrolytes, Li dendrites can be already seen with SEM, as shown in Figure 4a. Their presence can be indicated by F-signals at exactly these spots, because these intense F-signals can be regarded as representatives of intense LiPF₆-based decomposition products formed at previously highly reactive domains, for example, Li metal (dendrites). These domains are validated in our previous publication and could be attributed to Li dendrites by means of, for example, microscopic techniques and Li NMR.^[20] Moreover, these Li metal dendrites are obviously formed at the same spots, where

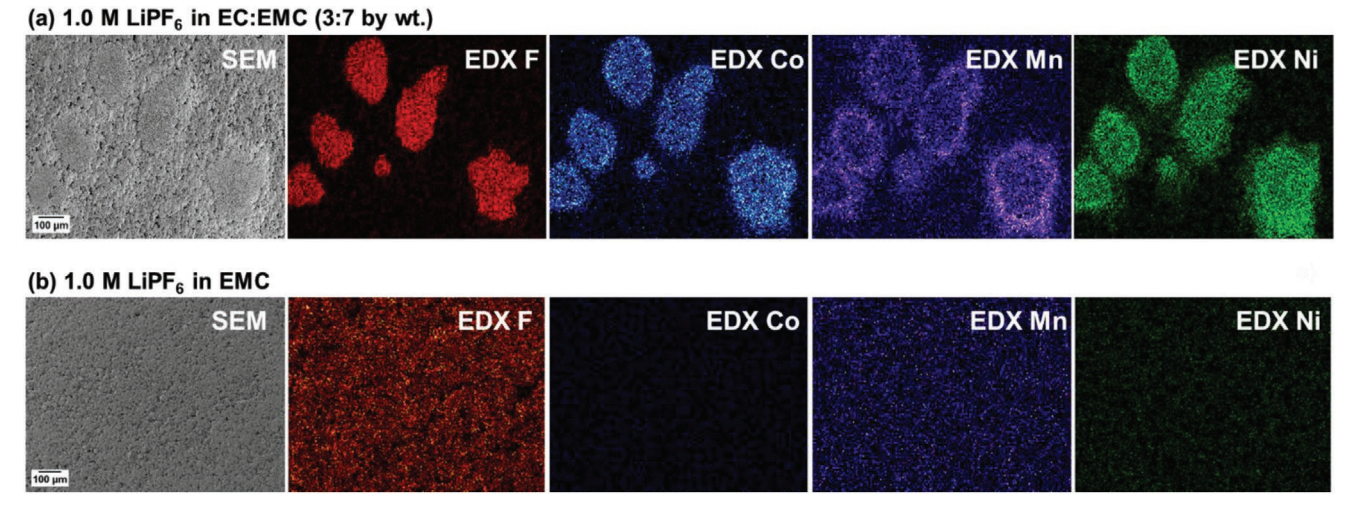


Figure 4. SEM-EDX images of graphite-based anodes after 100 charge/discharge cycles in Al_2O_3 -NCM523|graphite cells with a) EC-based and b) EC-free electrolytes. For EC-based electrolyte, Li dendrites and accumulated TMs can be observed and located at the same spots. Hence, Li dendrites as the proposed result of an electrode crosstalk are obviously suppressed in the EC-free electrolyte, as the spots of TMs and Li dendrites cannot be observed.

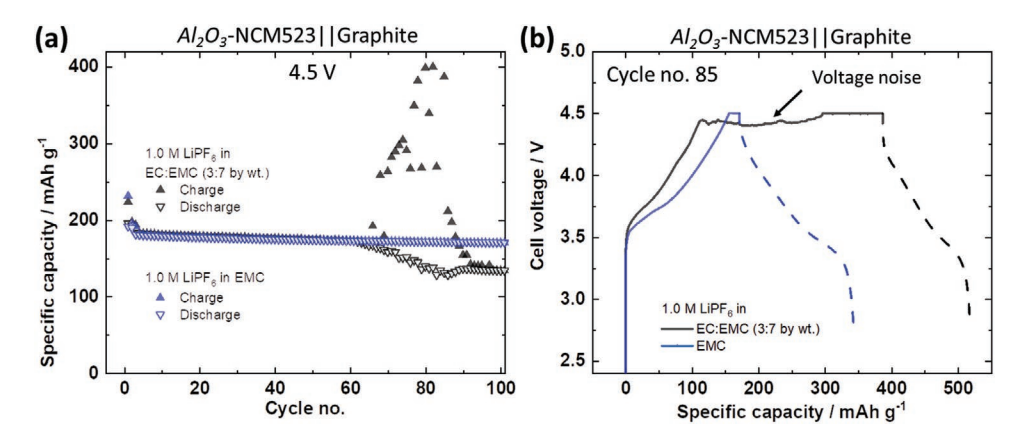


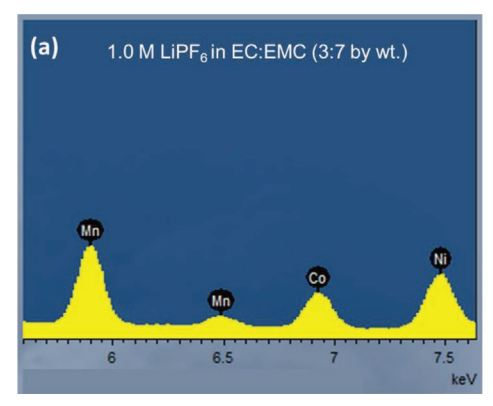
Figure 5. a) Specific charge and discharge capacities as a function of cycle number in Al_2O_3 -NCM523||graphite cells with EC-based and EC-free electrolytes. The significantly increased and random specific charge capacities of the EC-based electrolyte during rollover failure hint at penetration of Li metal dendrites. b) Initial charge process of the 85th cycle. The random voltage noise as indication for micro short-circuits is an additional hint for penetration of Li dendrites.

TM previously deposit, as they are located at identical spots as shown in the SEM-EDX analysis for Co, Mn, and Ni. Interestingly, the graphite-based anode cycled in the EC-free electrolyte is free of these spots based on TMs and Li metal dendrites.

The presence of Li metal dendrites and their association with the rollover failure can be additionally identified by electrochemical experiments, as shown in Figure 5. The charge/ discharge cycling of Al₂O₃-NCM523||graphite cells using the EC-based electrolyte abruptly results in a random increase of specific charge capacities, which correlates with the onset of rollover fading, as shown in Figure 5a. As known from, for example, Li metal batteries a sudden and random increase in specific charge capacity typically hints at penetrating Li dendrites, which results in micro short-circuits and subsequently raises the specific charge capacity.[44-47] In fact, a deeper look at the charging process of, for example, the 85th cycle, confirms these micro short-circuits via the characteristic noise in the voltage profile, as shown in Figure 5b. The formation of Li metal dendrites, which is a highly reactive morphology of metallic lithium due to its high surface area, [48-50] can be regarded as the source of rollover failure, as their presence is accompanied by significant losses of active Li, thus the specific capacity.^[51] In contrast, the EC-free electrolyte cell performs without any indications for Li dendrites.

Obviously, the TM deposits on graphite are the spots for subsequent Li dendrite growth, which has been thoroughly discussed in our previous publication. [20] To clarify their absence in EC-free electrolyte, the entire graphite-based anodes are analyzed with respect to the TM amount by means of EDX analysis and are depicted in **Figure 6**. In total, significantly more TMs are detected at the graphite surface after 100 cycles, when cycled with the EC-based electrolyte (Figure 6a) compared to graphite anodes cycled in the EC-free electrolyte (Figure 6b). The visualized spots of TMs in Figure 4a are obviously the result of different amounts of TM deposits and the detrimental mechanism is for EC-based electrolyte is summarized in **Scheme 1**. Finally, the superior cycle life of EC-free electrolytes can be concluded to be the result of suppressed detrimental crosstalk via suppressed mitigation of TMs toward the anode.

A salient difference between EC-based and EC-free electrolytes can be anticipated in the composition of the SEI layer on graphite, which is known to be sensitively influenced by electrolytes. [25,52–54] The SEI composition obtained by X-ray photoelectron spectroscopy (XPS) analysis is depicted in **Figure 7a**. Less organic- (e.g., carbonate) species are found in the SEI of EC-free electrolyte, which points to lower solvent decomposition compared to the EC-based electrolyte. Indeed, the portion of degraded LiPF₆ products is significantly higher for EC-free



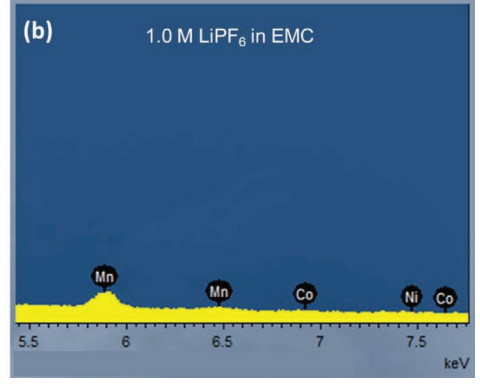
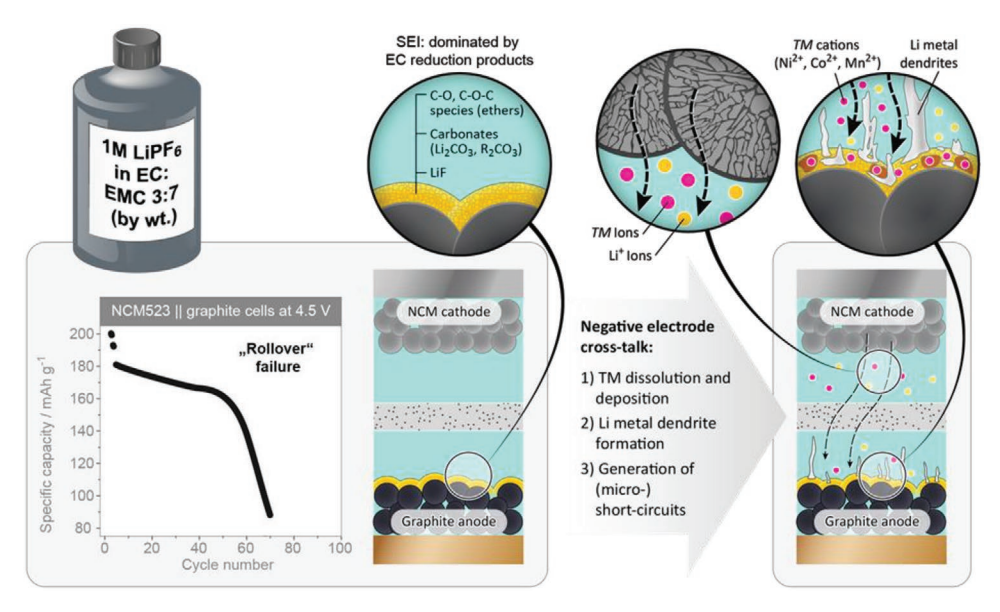


Figure 6. EDX for various TMs (Mn, Co, Ni) at the graphite-based anode after 100 charge/discharge cycles in Al_2O_3 -NCM523||graphite cells with a) EC-containing electrolyte and b) EC-free electrolyte. The use of EC-free electrolytes significantly reduces TM depositions on the graphite-based anode.



Scheme 1. Mechanism of rollover fading of EC-based electrolyte.

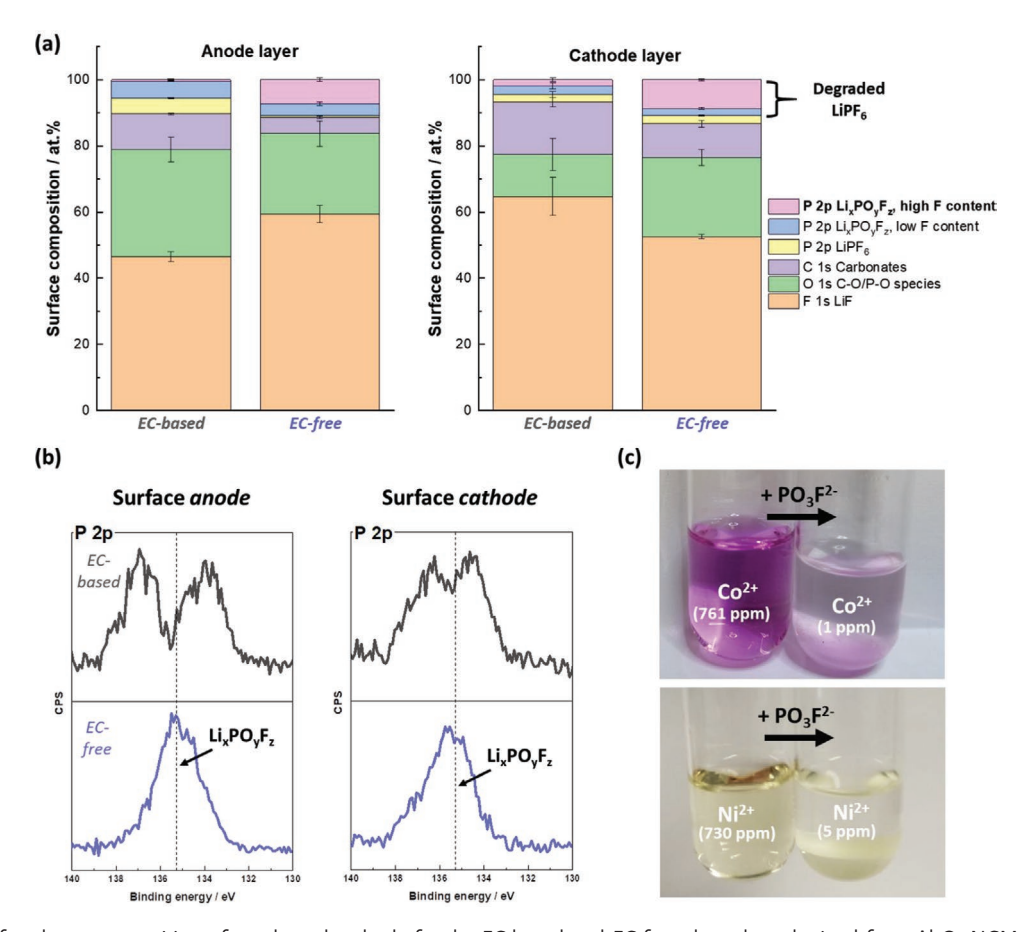


Figure 7. a) Surface layer composition of anode and cathode for the EC-based and EC-free electrolyte obtained from Al_2O_3 -NCM523|graphite cells after 100 cycles, showing more degraded LiPF₆ species on both electrodes for the EC-free electrolyte. b) Phosphorous 2p-spectra of the SEI and Al_2O_3 -NCM523 CEI. Enhanced presence of $Li_xPO_yF_z$ species can be concluded for the EC-free electrolyte on both electrodes. c) Precipitation experiments: the addition of an exemplary PO_3F^3 —based species to Ni^{2+} - and Co^{2+} -containing EC-based electrolyte significantly reduces the transition metal ion concentration. Given the higher amount of $Li_xPO_yF_z$ in EC-free electrolytes on both electrodes, the transition metals can be concluded to be reduced via scavenging effects.

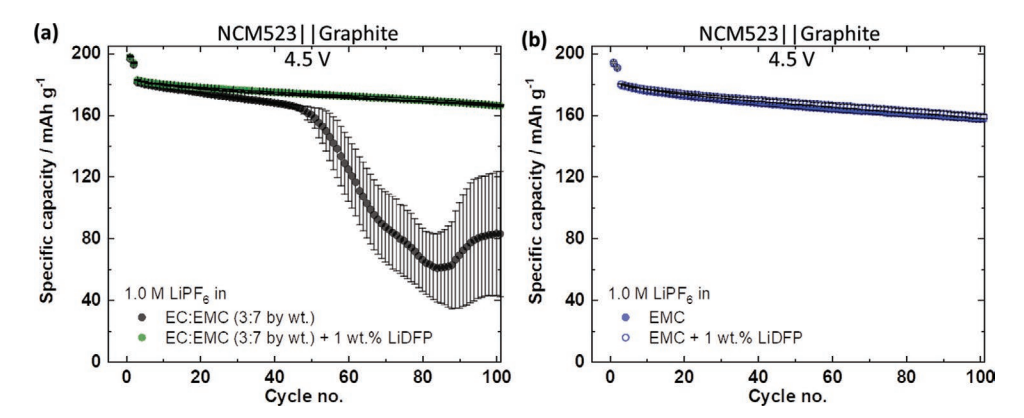


Figure 8. Charge/discharge cycling of NCM523||graphite full cells at 4.5 V for the electrolytes without and with the addition of 1 wt% LiDFP in a) The EC-based electrolyte and b) EC-free electrolyte. The presence of these phosphate additives indeed suppresses the rollover fading, while it has no significant effect on the EC-free electrolyte. This proves that the superior performance of EC-free electrolyte can be related with the generated phosphate-based species, which prevent the crosstalk and rollover failure.

electrolytes, which can be seen by an enhanced amount of Li_xPO_yF_z-based species, that are known to form in these electrolytes.^[55] These are present for the EC-free electrolyte on both electrodes. Slight amounts are also found for EC-based electrolytes, but the LixPOvFz composition is different for the EC-free electrolyte as seen by different binding energies in the P2p-spectra (Figure 7b). They can scavenge the dissolved TMs in the electrolyte, as exemplarily illustrated in Figure 7c for the EC-based electrolytes with extra added Co²⁺- and Ni²⁺, which are colored violet and yellow, respectively. For example, the addition of PO₂F²⁻, as an exemplary decomposition product of LiPF₆, significantly reduces the concentration of Co²⁺ and Ni²⁺, which is already visible by reduced color as well as analytically via ion chromatography (IC), also for the non-colored Mn²⁺ species, that is, the Co²⁺, Ni²⁺, and Mn²⁺ contents are reduced from \approx 761, \approx 730, and \approx 651 ppm, to \approx 1 ppm for Co²⁺ and Mn²⁺ and to ≈5 ppm for Ni²⁺, respectively.

The prevention of TM deposition at graphite via their complexation with Li_xPO_vF_z species can be concluded to be the underlying mechanism for the suppression of rollover failure for cells using EC-free electrolytes. This principle is proven in Figure 8 via an external addition of such species to the electrolyte. A prominent candidate is the additive lithium difluorophosphate (LiPO₂F₂; LiDFP), which also can be regarded as degraded LiPF₆ species and in fact can be generated in situ in the course of the aging reactions.[56-58] LiDFP is known to further decompose within the electrolyte to a variety of LixPOvFz species including PO₃F²—based species (Scheme 2). As shown in Figure 8a, the addition of 1 wt% LiDFP to the EC-based electrolyte can effectively suppress the rollover failure while its addition to the ECfree electrolyte has, as expected, no significant impact, which is shown in Figure 8b. Finally, the key difference regarding the shown high-voltage performance between the EC-based and ECfree electrolytes can be concluded to be the presence of Li_xPO_vF_z species, obviously acting as scavenger for TM species.

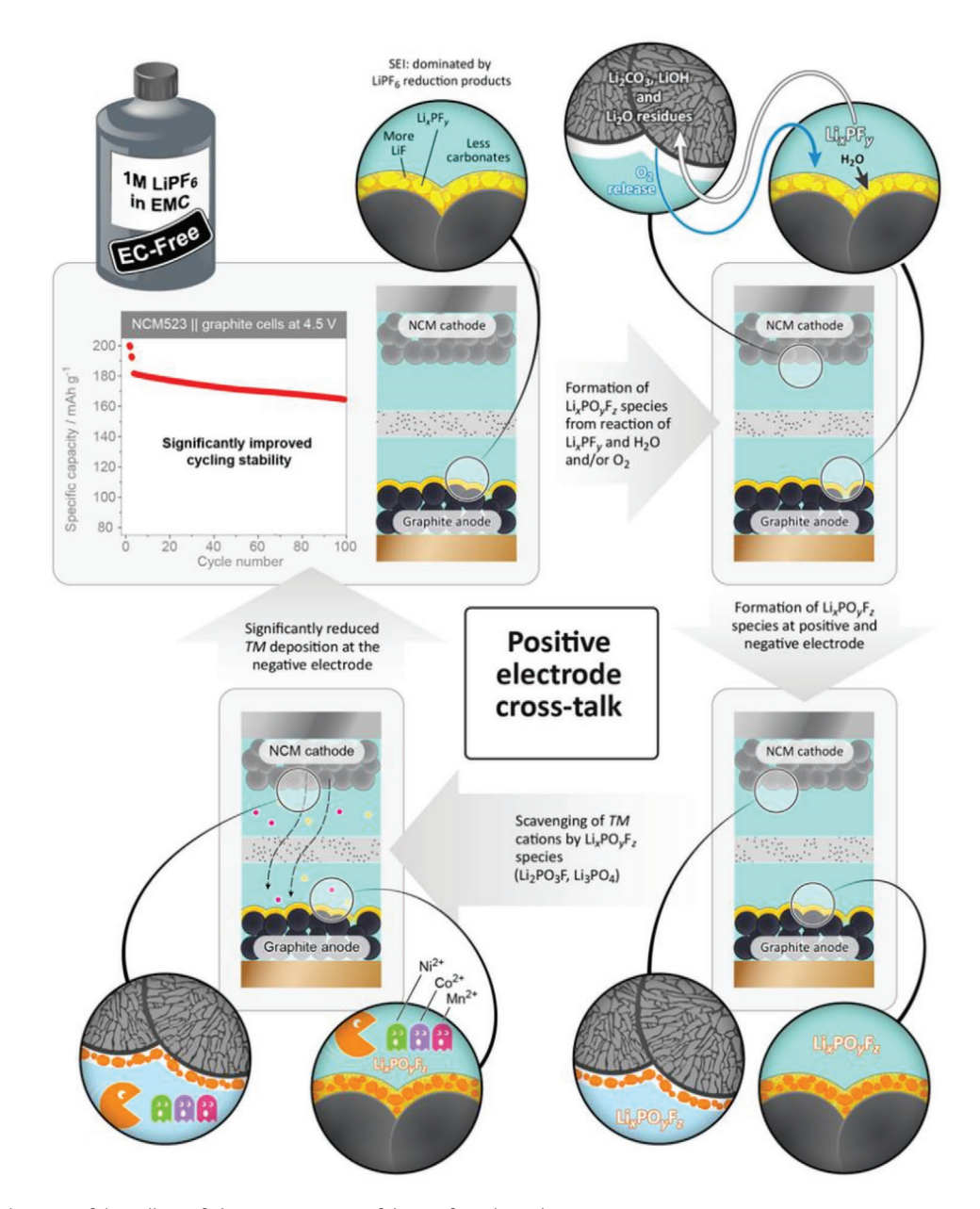
To sum up, the migration of the dissolved TM ions from the cathode to the anode, that is, (negative) crosstalk, initiates the rollover failure, as it leads to formation of dendritic Li and subsequent reaction with electrolyte, which finally leads to a loss of active Li and specific capacity, resulting in the rollover

failure. Crosstalk suppression can proceed via bonding the TM ions by a simple modification of the electrolyte. [20] The mechanistic difference of EC-free electrolyte compared to EC-based electrolyte (Scheme 1) is schematically illustrated in Scheme 2. Absence of the highly reductive EC[25,59,60] promotes reduction of LiPF₆ at graphite side resulting in more Li_rPF_v species.^[61,62] The contact with oxygen species (LiOH, Li₂CO₃, water traces, oxygen release from cathode, etc.)[63] finally generates the beneficial Li_xPO_yF_z-species, which are able to bond TM ions (e.g., via chelating complexation). Moreover, these species can migrate to the cathode side in the course of a beneficial (positive) crosstalk, that is, movement from anode to cathode, and directly bond the dissolved TM ions on the cathode side, thus directly prevent the detrimental (negative) crosstalk in its initial state. The addition of LiDFP as an electrolyte additive proofs the principle, as it suppresses the (detrimental and negative) crosstalk and rollover fading also for EC-based electrolytes. Additionally, the crosstalk suppression directly on cathode side also prevents the risk of several destabilizations and corrosion effects, which may occur due to continuously dissolving TM ions as recently reported. [64,65]

These species, in particular their various possible decomposition products, $^{[66]}$ are the key for the overall suppression of rollover fading, each with characteristic bonding ability. The thorough analysis, including precise solubility and bonding abilities of decomposed LiPF₆ species is part of our future work as it may support a more systematic R&D of, for example, additives. Additionally, more studies for this promising electrolyte may support its evaluation for application, including their limitations, which may occur due to lower ionic conductivity (high rate and/or low temperature performance, etc.).

3. Conclusions

The increase of cell voltage in LIBs, for example, of $\text{LiNi}_{0.5}\text{Co}_{0.2}\text{Mn}_{0.3}\text{O}_2$ (NCM523)||graphite cells is a promising strategy to increase energy density and the specific energy. However, this approach significantly limits the cycle life and in extreme cases, that is, > 4.5 V charge voltage, the cell suffers from the sudden and abrupt rollover failure when using SOTA



Scheme 2. Mechanism of the rollover fading suppression of the EC-free electrolyte.

electrolyte, that is, $1.0 \,\mathrm{m}$ LiPF₆ in a blend of cyclic EC and linear carbonate, for example, EMC. The rollover failure is a result of Li dendrite metal formation at graphite triggered in the course of electrode crosstalk, that is, TM dissolution from the cathode and then transport and deposition on the anode with a subsequent generation of micro short-circuits due to penetration of the lithium dendrites toward the cathode.

Interestingly, the elimination of EC from the SOTA electrolyte suppresses the rollover failure at 4.5 V. Obviously, EC is not only less vital for the physicochemical aspects than expected, as the electrolyte (e.g., $1.0~\rm M$ LiPF $_6$ in EMC) still reveals sufficient ionic conductivity and similar anodic stability, but is even disadvantageous for high voltage applications. By means of SEM and EDX it is shown that significantly less TMs and Li dendrites

are deposited on the anode for the EC-free electrolyte, while for the EC-based electrolyte intense TM deposits and Li dendrites can be visualized and even their penetration toward the cathode can be electrochemically observed via the characteristic voltage noise.

The beneficial effect, which is the suppressing ability of electrode crosstalk, thus the rollover failure, can be attributed to significantly higher amounts of degraded LiPF₆ species, that is, $\text{Li}_x \text{PO}_y \text{F}_z$, (e.g., LiDFP) as shown by means of XPS. As shown by precipitation experiments and analysis via IC-CD (CD: conductivity detection), these species can effectively scavenge TMs from the electrolyte and counteract the electrode crosstalk phenomenon. This principle is proven via addition of these species to SOTA, that is, EC-based, electrolyte. In fact, the addition of



www.advancedsciencenews.com

www.advenergymat.de

ADVANCED ENERGY MATERIALS

only 1 wt. % LiDFP realizes rollover-free charge/discharge cycle performance. This work not only demonstrates the significant practical benefit of EC-free electrolytes, but also the importance of $\text{Li}_x \text{PO}_v \text{F}_z$ species for high-voltage applications in LIB cells.

4. Experimental Section

Electrode Preparation: NCM523-based cathodes and graphitebased anodes were prepared in large-scale at an in-house battery line. The cathodes consisted of 95 wt% pristine polycrystalline NCM523 ("NCM523"; Custom Cells Itzehoe GmbH) or aluminum oxidecoated poly crystalline NCM523 ("Al₂O₃-NCM523"; Umicore), 3 wt% polyvinylidene difluoride (PVdF) binder (Solef 5130, Solvay), and 2 wt% carbon black (Super C65, Imerys Graphite & Carbon), and were cast onto aluminum foil (15 µm; Nippon Foil). The solvent for cathode manufacturing was N-methyl-2-pyrrolidone (NMP, Sigma Aldrich, purity: 99.5%). The anodes consisted of 95 wt% graphite (SG3, natural graphite, SGL Carbon), 1.5 wt% styrene-butadiene-rubber (SBR; SB5521, LIPATON, Polymer Latex GmbH), 3 wt% Na-CMC (Walocel CRT 2000 PPA12; Dow Wolff Cellulosics), and 0.5 wt% carbon black (Super C65. Imerys Graphite & Carbon) and were cast onto copper foil (10 μm; Nippon Foil), using deionized water as solvent. The anode mass loading was 8.8 mg cm⁻². After drying and calendaring (porosity: 30%), the electrode sheets were punched into circular Ø14 mm (cathode) and Ø15 mm (anode) discs, and further dried in a vacuum oven at 100 °C under reduced pressure. The electrode capacity balancing of anode and cathode (N:P ratio) was set to ≈1.35:1.00 for the p-NCM523 || graphite cells and ≈1.40:1.00 for the Al₂O₃-NCM523 || graphite cells at 4.5 V. LNMO (Johnson Matthey) is self-made with a ratio of active material, SuperC, PVDF5130 of 85:10:5 and a capacity loading of ≈0.5 mAh cm⁻².

Electrolyte Preparation: The standard electrolytes used in this work were 1 $\,\rm M$ LiPF $_6$ in EC:EMC 3:7 (by weight; "STD" electrolyte; Solvionic; purity: battery grade) and 1 $\,\rm M$ LiPF $_6$ in EMC ("EC-free" electrolyte; Sigma Aldrich, purity: battery grade). In another experiment, 1.0 wt% of the electrolyte additive LiDFP (American Elements; CAS No.: 24389-25-1; purity: ≥99.9%) was added to the STD and EC-free electrolytes.

To investigate the interaction of, for example, Na_2PO_3F and dissolved Ni^{2+} , Mn^{2+} and Co^{2+} cations, 10 mg of $Ni(TFSI)_2$ (Alfa Aesar; CAS No.: 207861-63-0), 10 mg of $Co(TFSI)_2$ (Alfa Aesar; CAS No.: 207861-61-8) and 10 mg of $Mn(TFSI)_2$ (Alfa Aesar; CAS No.: 2070861-55-0) were each dissolved in 1 mL of the "STD" electrolyte.

From IC analysis, ≈ 750 ppm of Ni²+, Co²+, and 650 ppm Mn²+ were found in the electrolyte. Afterward, 100 mg of Na²PO³F (Sigma Aldrich; CAS No.: 10163-15-2; purity: 95%) was added to each of the electrolytes and left for 24 h at 20 °C. The precipitated solids were separated from the electrolyte solution by filtration.

Cell Assembly: 2032-type coin cells (two-electrode configuration) $^{[38]}$ were assembled to investigate TM dissolution from the NCM523 cathode and the TM deposition at the graphite anode in NCM523 \parallel graphite full-cells. The Ø15 mm anode disc was separated by a Celgard 2500 separator (polypropylene, one layer) from the Ø14 mm cathode disc, which was soaked with 40 μ L of the electrolyte. The overcharge experiment was conducted in a three-electrode cell set-up with Li as reference- and counter electrode and LNMO as working electrode. $^{[38,67]}$ The cut-off potential was set to 6 V versus Li|Li+ using a current of 0.12 mA.

Constant Current-Constant Voltage Charge/Discharge Cycling: The electrochemical charge/discharge cycling performance of NCM523 \parallel graphite full-cells was studied via constant current charge/discharge cycling on a Maccor 4000 battery testing system in cell voltage ranges between 2.8 and 4.5 V. The cell formation conditions consisted of one cycle at 0.1 C and one cycle at 0.2 C. Afterward, the cells were cycled with 1 C (1 C = 190 mA g⁻¹ at 4.5 V). After each charging step, a constant voltage step was performed with the limiting conditions of either achieving a time limit of maximal 30 min, or when the specific current reaches values below 0.05 C. All electrochemical studies were performed

in climatic chambers at 20 $^{\circ}$ C. At least three cells were evaluated for each study to ensure high reproducibility, which is indicated by error bars in the respective Figures.

SEM and EDX Spectroscopy Investigations of Graphite Anodes after Cycling: The investigation of the surface morphology of the cycled graphite anodes (after 100 cycles) was performed by a Zeiss Auriga electron microscope and EDX was carried out with an accelerating voltage of 20 kV with an EDX detector (X-MaxN 80 mm², Oxford Instruments). Prior to analysis, the cells were disassembled in dry atmosphere (dry room) and the anode surfaces were rinsed with 1 mL of EMC. After a short drying period under reduced pressure, the electrodes were transferred into the SEM advice via a vacuum sealed sample holder to avoid any contact with moisture.

XPS Investigations of Graphite Anodes after Cycling: XPS samples were mounted on a sample holder and transported to a glovebox connected to an Axis Ultra DLD XPS (Kratos Analytical). From here, samples were moved into an ultra-high vacuum (10-8 mbar) chamber inside the device. Here, samples were stored for at least 12 h to remove volatile species, before moving the samples into the analysis chamber. XPS was measured using a monochromatic Al K α source (hv = 1486.6 eV) at an emission current of 10 mA and with an accelerating voltage of 12 kV. A charge neutralizer was used to suppress positive charging of the sample's surface. A small area spectroscopy aperture of 110 μm was used for the core spectra of the graphite anodes. The angle of emission was 0° and the hemispherical analyzer was set to a pass energy of 160 eV for survey spectra and 40 eV for graphite anode core spectra. Core spectra were recorded in the following regions: F 1s, O 1s, C 1s, P 2p, and Li 1s.

IC-CD Investigations TM Cations: IC was performed on an 850 Professional IC (Metrohm, Herisau, Switzerland) comprising a chemical suppressor and CD. Cations were separated on a Metrosep C6-250/4.0 column on a Compact IC Pro 881 instrument (Metrohm, Herisau, Switzerland) with CD. A sample volume of 200 μ L was separated at 40 °C with an isocratic 0.85 mm oxalic acid/4.15 mm nitric acid eluent. The method and sample preparation were based on Vortmann–Westhoven et al. $^{[68]}$ Both IC systems were controlled with MagIC NetTM 3.2.

Acknowledgements

The authors wish to thank the Federal Ministry for Economic Affairs and Energy (BMWi) for funding this work in the project "Go3" (03ETE002D). The authors also thank Andre Bar for his graphical support.

Open access funding enabled and organized by Projekt DEAL.

Conflict of Interest

The authors declare no conflict of interest.

Data Availability Statement

Data available on request from the authors.

Keywords

conventional electrolytes, ethylene carbonate-free, high voltage, Li ion batteries, rollover fading

Received: December 1, 2020 Revised: January 18, 2021 Published online: January 29, 2021

^[1] J. B. Goodenough, Y. Kim, J. Power Sources 2011, 196, 6688.

^[2] R. Schmuch, R. Wagner, G. Hörpel, T. Placke, M. Winter, Nat. Energy 2018, 3, 267.

- [3] M. Winter, B. Barnett, K. Xu, Chem. Rev. 2018, 118, 11433.
- [4] J. B. Goodenough, K. S. Park, J. Am. Chem. Soc. 2013, 135, 1167.
- [5] J. Kasnatscheew, M. Evertz, R. Kloepsch, B. Streipert, R. Wagner, I. Cekic Laskovic, M. Winter, Energy Technol. 2017, 5, 1670.
- [6] J. Kasnatscheew, S. Röser, M. Börner, M. Winter, ACS Appl. Energy Mater. 2019, 2, 7733.
- [7] J. Kasnatscheew, M. Evertz, B. Streipert, R. Wagner, S. Nowak, I. Cekic Laskovic, M. Winter, J. Power Sources 2017, 359, 458.
- [8] A. Manthiram, Nat. Commun. 2020, 11, 1550.
- [9] I. Buchberger, S. Seidlmayer, A. Pokharel, M. Piana, J. Hattendorff, P. Kudejova, R. Gilles, H. A. Gasteiger, J. Electrochem. Soc. 2015, 162, A2737.
- [10] J. A. Gilbert, I. A. Shkrob, D. P. Abraham, J. Electrochem. Soc. 2017, 164, A389.
- [11] H. Zheng, Q. Sun, G. Liu, X. Song, V. S. Battaglia, J. Power Sources 2012, 207, 134.
- [12] D. P. Abraham, T. Spila, M. M. Furczon, E. Sammann, Electrochem. Solid-State Lett. 2008, 11, A226.
- [13] T. Joshi, K. Eom, G. Yushin, T. F. Fuller, J. Electrochem. Soc. 2014, 161. A1915.
- [14] M. Ochida, Y. Domi, T. Doi, S. Tsubouchi, H. Nakagawa, T. Yamanaka, T. Abe, Z. Ogumi, J. Electrochem. Soc. 2012, 159, A961.
- [15] O. C. Harris, S. E. Lee, C. Lees, M. Tang, J. Phys.: Energy 2020, 2, 032002.
- [16] C. Zhan, T. Wu, J. Lu, K. Amine, Energy Environ. Sci. 2018, 11, 243.
- [17] X. Ma, J. E. Harlow, J. Li, L. Ma, D. S. Hall, S. Buteau, M. Genovese, M. Cormier, J. R. Dahn, J. Electrochem. Soc. 2019, 166, A711.
- [18] L. Madec, L. Ma, K. J. Nelson, R. Petibon, J.-P. Sun, I. G. Hill, J. R. Dahn, J. Electrochem. Soc. 2016, 163, A1001.
- [19] R. S. Arumugam, L. Ma, J. Li, X. Xia, J. M. Paulsen, J. R. Dahn, J. Electrochem. Soc. 2016, 163, A2531.
- [20] S. Klein, P. Bärmann, T. Beuse, K. Borzutzki, J. Frerichs, J. Kasnatscheew, M. Winter, T. Placke, ChemSusChem 2020, https://doi.org/10.1002/cssc.202002113.
- [21] P. Janssen, J. Kasnatscheew, B. Streipert, C. Wendt, P. Murmann, M. Ponomarenko, O. Stubbmann-Kazakova, G.-V. Röschenthaler, M. Winter, I. Cekic-Laskovic, J. Electrochem. Soc. 2018, 165, A3525.
- [22] J. Kasnatscheew, R. W. Schmitz, R. Wagner, M. Winter, R. Schmitz, J. Electrochem. Soc. 2013, 160, A1369.
- [23] T. Dagger, J. Kasnatscheew, B. Vortmann-Westhoven, T. Schwieters, S. Nowak, M. Winter, F. M. Schappacher, J. Power Sources 2018, 396, 519
- [24] J. Kasnatscheew, T. Placke, B. Streipert, S. Rothermel, R. Wagner, P. Meister, I. C. Laskovic, M. Winter, J. Electrochem. Soc. 2017, 164, A2479.
- [25] K. Xu, Chem. Rev. 2004, 104, 4303.
- [26] K. Xu, S. P. Ding, T. R. Jow, J. Electrochem. Soc. 1999, 146, 4172.
- [27] L. Ma, S. L. Glazier, R. Petibon, J. Xia, J. M. Peters, Q. Liu, J. Allen, R. N. C. Doig, J. R. Dahn, J. Electrochem. Soc. 2016, 164, A5008.
- [28] R. Petibon, J. Xia, L. Ma, M. K. G. Bauer, K. J. Nelson, J. R. Dahn, J. Electrochem. Soc. 2016, 163, A2571.
- [29] J. Xia, R. Petibon, D. Xiong, L. Ma, J. R. Dahn, J. Power Sources 2016, 328, 124.
- [30] W. Li, A. Dolocan, J. Li, Q. Xie, A. Manthiram, Adv. Energy Mater. 2019, 9, 1901152.
- [31] Q. Q. Liu, D. J. Xiong, R. Petibon, C. Y. Du, J. R. Dahn, J. Electrochem. Soc. 2016, 163, A3010.
- [32] J. Xia, S. L. Glazier, R. Petibon, J. R. Dahn, J. Electrochem. Soc. 2017, 164, A1239.
- [33] J. Hoffmann, M. S. Milien, B. L. Lucht, M. Payne, J. Electrochem. Soc. 2018, 165, A3108.
- [34] J. Kasnatscheew, U. Rodehorst, B. Streipert, S. Wiemers-Meyer, R. Jakelski, R. Wagner, I. C. Laskovic, M. Winter, J. Electrochem. Soc. 2016, 163, A2943.

[35] J. Kasnatscheew, M. Evertz, B. Streipert, R. Wagner, R. Klopsch, B. Vortmann, H. Hahn, S. Nowak, M. Amereller, A. C. Gentschev, P. Lamp, M. Winter, Phys. Chem. Chem. Phys. 2016, 18, 3956.

ENERGY

- [36] J. Kasnatscheew, B. Streipert, S. Röser, R. Wagner, I. Cekic Laskovic, M. Winter, Phys. Chem. Chem. Phys. 2017, 19, 16078.
- [37] B. Streipert, L. Stolz, G. Homann, P. Janßen, I. Cekic-Laskovic, M. Winter, J. Kasnatscheew, ChemSusChem 2020, 13, 5301.
- [38] R. Nölle, K. Beltrop, F. Holtstiege, J. Kasnatscheew, T. Placke, M. Winter, Mater. Today 2020, 32, 131.
- [39] J. C. Burns, A. Kassam, N. N. Sinha, L. E. Downie, L. Solnickova, B. M. Way, J. R. Dahn, J. Electrochem. Soc. 2013, 160, A1451.
- [40] C. Zhang, Y. Wang, Y. Gao, F. Wang, B. Mu, W. Zhang, Appl. Energy 2019, 256, 113841.
- [41] W. Liu, X. Li, D. Xiong, Y. Hao, J. Li, H. Kou, B. Yan, D. Li, S. Lu, A. Koo, K. Adair, X. Sun, Nano Energy 2018, 44, 111.
- [42] G. Cao, Z. Jin, J. Zhu, Y. Li, B. Xu, Y. Xiong, J. Yang, J. Alloys Compd. 2020, 832, 153788.
- [43] Y. Shi, M. Zhang, D. Qian, Y. S. Meng, Electrochim. Acta 2016, 203, 154.
- [44] G. Homann, L. Stolz, M. Winter, J. Kasnatscheew, iScience 2020, 23, 101225
- [45] G. Homann, L. Stolz, J. Nair, I. C. Laskovic, M. Winter, J. Kasnatscheew, Sci. Rep. 2020, 10, 4390.
- [46] G. Homann, L. Stolz, K. Neuhaus, M. Winter, J. Kasnatscheew, Adv. Funct. Mater. 2020, 30, 2006289.
- [47] G. Homann, P. Meister, L. Stolz, J. P. Brinkmann, J. Kulisch, T. Adermann, M. Winter, J. Kasnatscheew, ACS Appl. Energy Mater. 2020, 3, 3162.
- [48] C. Brissot, M. Rosso, J. N. Chazalviel, S. Lascaud, J. Power Sources 1999, 81, 925.
- [49] P. Bai, J. Li, F. R. Brushett, M. Z. Bazant, Energy Environ. Sci. 2016, 9, 3221.
- [50] G. Bieker, M. Winter, P. Bieker, Phys. Chem. Chem. Phys. 2015, 17, 8670
- [51] F. Holtstiege, A. Wilken, M. Winter, T. Placke, Phys. Chem. Chem. Phys. 2017, 19, 25905.
- [52] R. Fong, U. von Sacken, J. R. Dahn, J. Electrochem. Soc. 1990, 137, 2009
- [53] K. Xu, A. von Cresce, J. Mater. Chem. 2011, 21, 9849.
- [54] P. Niehoff, S. Passerini, M. Winter, Langmuir 2013, 29, 5806.
- [55] S. Nowak, M. Winter, J. Electrochem. Soc. 2015, 162, A2500.
- [56] S. Klein, K. Borzutzki, P. Schneider, O. Fromm, J. Reiter, Q. Fan, T. Placke, M. Winter, J. Kasnatscheew, Chem. Mater. 2020, 32, 6279.
- [57] G. G. Botte, R. E. White, Z. M. Zhang, J. Power Sources 2001, 97, 570.
- [58] C. L. Campion, W. T. Li, B. L. Lucht, J. Electrochem. Soc. 2005, 152, A2327.
- [59] R. Gauthier, D. S. Hall, T. Taskovic, J. R. Dahn, J. Electrochem. Soc. 2019, 166, A3707.
- [60] A. Wang, S. Kadam, H. Li, S. Shi, Y. Qi, npj Comput. Mater. 2018, 4, 15.
- [61] B. S. Parimalam, B. L. Lucht, J. Electrochem. Soc. 2018, 165, A251.
- [62] J. Kasnatscheew, R. Wagner, M. Winter, I. Cekic-Laskovic, Top. Curr. Chem. 2018, 376, 16.
- [63] J. Kasnatscheew, M. Evertz, B. Streipert, R. Wagner, S. Nowak, I. Cekic Laskovic, M. Winter, J. Phys. Chem. C 2017, 121, 1521.
- [64] C. Wang, L. Xing, J. Vatamanu, Z. Chen, G. Lan, W. Li, K. Xu, Nat. Commun. 2019, 10, 3423.
- [65] X.-Q. Zhang, X.-M. Wang, B.-Q. Li, P. Shi, J.-Q. Huang, A. Chen, Q. Zhang, J. Mater. Chem. A 2020, 8, 4283.
- [66] S. Klein, P. Harte, J. Henschel, P. Baermann, K. Borzutzki, T. Beuse, S. Van Wickeren, B. Heidrich, J. Kasnatscheew, S. Nowak, M. Winter, T. Placke, Adv. Energy Mater. 2020, https://doi. org/10.1002/aenm.202003756.
- [67] J. Kasnatscheew, M. Börner, B. Streipert, P. Meister, R. Wagner, I. Cekic Laskovic, M. Winter, J. Power Sources 2017, 362, 278.
- [68] B. Vortmann-Westhoven, M. Diehl, M. Winter, S. Nowak, Chromatographia 2018, 81, 995.